Development of Fe-promoted Ni-Al catalyst for hydrogen production from gasification of wood sawdust

Lisha Dong [a], Chunfei Wu [b*], Huajuan Ling [a], Jeffrey Shi [a], Paul T. Williams [c,*], Jun Huang [a,*]
[a] Laboratory for Catalysis Engineering, School of Chemical and Biomolecular Engineering, The University of Sydney, NSW 2006, Australia
(Tel: #61 2 9351 7483; Email: jun.huang@sydney.edu.au)
[b] School of Engineering, The University of Hull, Hull HU6 7RX, UK
(Tel: #44 1482 466464; Email: c.wu@hull.ac.uk)
[c] School of Chemical & Process Engineering, The University of Leeds, LS2 9JT, UK
(Tel: #44 1133432504; Email: p.t.williams@leeds.ac.uk)

ABSTRACT:

The production of renewable hydrogen enriched gas from biomass waste is a promising technology for the development of a sustainable economy and society. Until now, there are still challenges of the technology in terms of the efficiency of hydrogen production. Catalyst is known and has been tested to enhance hydrogen production from biomass gasification. In particular using Ni-based catalysts, which have high reactivity for hydrogen production and are cost effective. However, developing a Ni-based catalyst with high thermal stability and resistance of coke deposition on the surface of the catalyst is still a challenging topic. In this work, Ni-Al catalysts doped with low-cost Fe metal were investigated for hydrogen enriched syngas production from gasification of biomass using a two-stage fixed bed reactor. NiO-Fe_2O_3-Al_2O_3 catalysts with various Ni:Fe molar ratios (9:1, 8:2, 6:4, 5:5, 4:6, 2:8 and 1:9) were studied aiming to understand the influence of Fe addition on the production of hydrogen and the catalyst stability in terms of coke deposition on surface. X-ray diffraction (XRD), temperature programme reduction (TPR) and Transmission electron microscopy (TEM) analysis of the fresh catalysts showed that nanoparticles (mainly $NiAl_2O_4$ spinel phase and Al_2O_3, ~5 nm) were identified in the catalysts. High dispersion of metal particles was obtained using a co-precipitation method of catalyst preparation. With the increase of Fe addition, hydrogen production was reduced from around 11 to 8 (mmol H_2 g^{-1} biomass). However, the addition of Fe into the Ni-based catalyst significantly reduced the amount of coke deposited on the surface of the catalyst. H_2/CO molar ratio was maximized to 1.28 when Ni:Fe molar ratio was 1:1. In addition, sintering of metal particles was not observed through the TEM analysis of the fresh and reacted catalyst.

1. Introduction

At present, fossil-based fuels, such as petroleum, coal, and natural gas, are used for over three quarters of the primary energy consumption in the world [1]. Due to the depletion of resources and the release of greenhouse gases, significant concerns have been raised on the utilization of fossil fuels in regard to energy security and environmental impacts [2]. The development of renewable and clean alternative energy sources is, therefore, deemed to be vital to address the current increasing demand for energy and to decrease environmental impacts of energy consumption [3, 4]. Currently, alternatives to fossil fuels are renewable fuels, i.e. biomass, hydropower and solar energy [5]. Biomass has attracted increasing attention since it is renewable, carbon neutral, and a wide range of cheap and non-food feedstocks are available.

Hydrogen-enriched syngas production from biomass via the gasification process is a promising technology [6]. Also, hydrogen is an ideal clean fuel source for low carbon energy systems [7, 8] and can be used directly in fuel cells [6]. Hydrogen has also been identified as an ideal energy carrier for other resources, such as hydropower, wind, solar and biomass [2, 9]. For example, the electricity generated from wind and hydropower can be converted into hydrogen through electrolysis in the purpose of energy storage. Furthermore, hydrogen-rich syngas production from biomass would result in the decrease of dependence on energy production from fossil fuels and, simultaneously, in the reduction of greenhouse gas emissions [10].

Hydrogen-rich syngas production from biomass gasification receives extensive attention from both industrial and academic researchers due to the high conversion efficiency [6, 11]. A challenge towards H_2 production from biomass gasification on a large scale is the formation of coke and tar which can be eliminated by thermal cracking (gasification at high temperature) or by the utilization of a catalyst (catalytic gasification) [6]. Particularly, in the presence of steam and catalyst, gas and hydrogen yields can be significantly enhanced because of the promotion of steam reforming and water-gas shift reactions [6].

It is known that Ni is an excellent element for steam gasification reactions and preferred as a catalytic active site than precious metal such as Pt, Rh and Ru, as Ni-based catalysts are relatively cheap and have high catalytic activities for hydrogen production [12, 13]. A number of catalyst supports (e.g. MCM-41, Mg-Al and Cu-Al) [2, 4, 14-16] have been tested for biomass gasification. Among them, Al_2O_3 is regarded as an effective support, in particular, in terms of the catalytic activity for hydrogen production and thermal stability [17, 18]. It has been reported that the addition of CeO_2 to Ni-catalysts enhanced the catalytic performance, and the formation of the Ni-CeO_2 nanocomposite was responsible for the high catalytic activity and high

resistance to coke formation [12, 18-20]. However, the cost of Ce species is quite high. It is proposed that Fe species have similar high redox properties as Ce-species and can help promote hydrogen production in the steam gasification of biomass [21]. The addition of Fe in the catalyst can significantly influence the gasification efficiency [6, 22-25]. For example, it was reported that Fe species promoted water-gas shift, reforming and decomposition reactions during the steam gasification of biomass [6, 21].

Both metallic Ni- and Fe- based catalysts as well as Ni-Fe bimetallic catalysts have been used in biomass gasification processes for tar elimination [26-28]. Ramli et al. [26] studied the production of hydrogen from steam gasification of palm kernel shell (PKS). In their work, zeolite β (BEA) supported bimetallic Fe and Ni catalysts have been prepared using a sequential impregnation method and calcined at temperatures between 500 and 700 ºC. It is reported that a strong interaction between Ni and Fe was observed at higher calcination temperatures (700 °C) resulting in the stabilization of Fe^{3+} and Ni^{2+} ions in the lattice, and thus a higher yield of hydrogen was produced due to the promoting of the water-gas shift reaction. Ni-Fe/α-Al_2O_3 bimetallic catalysts prepared by co-impregnation method have been investigated for the reforming of tar from the pyrolysis of cedar wood using a laboratory-scale continuous feeding dual-bed reactor at 550ºC [28]. The Ni loading amount was 12wt.%, and Fe was added with a Fe/Ni molar ratio between 0.13 and 2. It was reported that the surface of Fe atoms supplied oxygen species and the addition of Fe to Ni/α-Al_2O_3 enhanced the catalytic performance regarding the production of gas and the suppression of coke deposition on the surface of the catalyst. However, excess addition of Fe decreased the catalytic activity by decreasing the amount of surface Ni atoms [28].

There are few reports using Ni-Fe bimetallic catalyst for gasification of real biomass. In this work, co-precipitated NiO-Fe_2O_3-Al_2O_3 catalysts were prepared and investigated for hydrogen production from catalytic steam reforming of vapours derived from the pyrolysis of wood sawdust. It is aimed to develop an efficient catalyst for hydrogen production from biomass gasification in relation to the yield of hydrogen and the stability of catalyst (e.g. less coke formation on the surface of the catalyst and the prohibition of metal sintering). In particular, various molar ratios between Fe and Ni (1:9, 2:8, 4:6, 5:5, 6:4, 8:2 and 9:1) were studied, while the molar content of Al (support) was kept constant at 80%.

2. Experimental

2.1. Materials

Wood sawdust was used as raw biomass material, which has been reported in our previous report [29]. Proximate analysis of the biomass sample showed that the sample contains about 6.4 wt.% moisture, 74.8 wt.% volatiles, 18.3 wt.% fixed carbon and 1.2 wt.% ash. Additionally, an element analysis showed that the biomass sample has 5.9 wt.% of hydrogen, 47.1 wt.% of carbon, 0.1 wt.% of nitrogen and 46.9 wt.% of oxygen (obtained from mass difference).

NiO-Fe_2O_3-Al_2O_3 catalysts with various Ni:Fe molar ratios (9:1, 8:2, 6:4, 5:5, 4:6, 2:8 and 1:9) were synthesized using a co-precipitation method, when the molar amount of Al molar was kept constant at 80%. It is noted that the molar ratio of Ni and Fe in the catalyst was fixed at 20%. During the preparation of catalyst, certain amounts of $Ni(NO_3)_2 \cdot 6H_2O$, $Fe(NO_3)_3 \cdot 9H_2O$, $Al(NO_3)_3 \cdot 9H_2O$ were dissolved in deionized water. $NH_3 \cdot H_2O$ solution (2 mol L^{-1}) was slowly added to the above mixture to reach a pH value of 8. The suspension was kept at 60 ^oC within a water bath for one hour with continuously stirring. Filtration of the suspension was carried out afterward and the filtration cake was repeatedly washed with deionized water until a pH value of 7 was reached. The derived catalyst precursor was dried in an oven at 80^oC for about 10 h, followed by calcination at 800 ^oC for 4 h within static air (heating rate was 1 ^oC min^{-1}). Finally, the catalyst was ground to small particles with a size between 50 and 180 μm, and assigned as fresh catalyst.

2.2. Reaction system for catalytic steam biomass gasification

A two-stage fixed bed reaction system was used to test the developed catalysts for hydrogen production. The reaction system has been reported in our previous work [29]. In general, the biomass sample (wood sawdust) was pyrolyzed in a first reactor, and the derived vapours excluding the bio-char (retained in the first reactor) passed through a second reactor where catalyst and steam were presented to produce hydrogen-enriched syngas.

For each experiment, 0.25 g fresh catalyst (non-reduced) and 0.8 g biomass sample were used. Steam was generated by injecting water into the second reactor using a syringe pump. The water injection rate was 4.74 g h^{-1}. Carrier gas (N_2) with a flow rate of 80 ml min^{-1} was introduced into the reaction system before heating the reactors. The second reactor was initially heated to 800 °C, then the first reactor was heating to 535^oC with a heating rate of 40 $^{\circ}C$ min^{-1}. The products derived from the second reactor were introduced into a condensation system including an air cooled condenser and a dry-ice cooled condenser. The non-condensable gases were collected using a 25L Tedlar^{TM} gas bag.

The products (solid char residue and gas) and also the mass balance were obtained using the following equations. It is noted that the collected liquid contained both oil product and un-reacted water. In addition, hydrogen-enriched gas was the main product. Thus oil production was not evaluated in this work.

$$Gas\ yield\ (wt.\%) = \frac{\text{Weight of gas}}{\text{Weight of biomass sample + water of injected water}} \times 100 \qquad \text{Equation (1)}$$

$$Char\ residue\ yield\ (wt.\%) = \frac{\text{Weight of char residue}}{\text{Weight of biomass sample + water of injected water}} \times 100 \qquad \text{Equation (2)}$$

$$Mass\ balance = \frac{\text{Weight of char residue, gas and liquid}}{\text{Weight of biomass sample + water of injected water}} \times 100 \qquad \text{Equation (3)}$$

2.3. Gas analysis and characterisations of catalysts

2.3.1. Gas analysis

Concentrations of the non-condensable gases mainly including C_{1}-$_{4}$ hydrocarbons, CO, CO_2, H_2 and N_2 were analysed by gas chromatography (GC) (Varian 3380). A flame ionization detector (FID) and an 80-100 mesh HayeSep column were used to detect C_1 to C_4 hydrocarbon gases (N_2 as carrier gas). Thermal conductivity detector and a HayeSep 80-100 mesh column were used to determine the concentrations of CO, CO_2, H_2 and N_2. It is noted that calibrations were carried out to all the mentioned gases (argon as carrier gas).

2.3.2. Characterisations of catalysts

The surface area of the prepared catalyst was analysed in this work. During the analysis, nitrogen gas was used as the adsorbate, and the specific surface area of the fresh catalyst was determined by N_2 adsorption isotherms on a Quantachrome Autosorb-1 Instrument. Before the isotherm analysis, about 150 mg of catalyst was loaded and degassed under vacuum at 150 ˚C for 5 hours, and the surface area was then measured under liquid nitrogen. Five points within a P/P_0 range from 0.05 to 0.25 were collected, and the specific surface area was calculated using the five-point BET method.

Temperature programmed reduction of the prepared catalysts was carried out using a modified thermogravimetric analyzer (SDT Q600). Fresh catalyst was loaded in an alumina pan and placed in the thermogravimetric analyzer furnace. The furnace reaction area was purged by a flow containing 15% H_2 and 85% N_2 with a 100mL min^{-1}. The catalysts were heated from room temperature to 1200^{o}C at a rate of 10^{o}C min^{-1}.

Temperature-programmed oxidation (TPO) of reacted catalysts was carried out using a Stanton-Redcroft thermogravimetric analyzer to determine the properties and the weight of the coked carbons deposited on the surface of reacted catalysts. About ~~10~~ 25 mg of reacted catalyst was heated in an atmosphere of air with a heating rate of 15^{o}C min^{-1} to a final temperature of 800 °C.

Catalysts were also analysed using scanning electron microscopy (SEM) (LEO 1530) and transmission electron microscopy (TEM) (Philips CM120 BioFilter) to obtain detailed morphologies of fresh and reacted catalysts. In addition, X-ray diffraction (XRD) was also carried out to the fresh catalysts. During the XRD analysis, a SIEMENS D5000 equipment was used in a range of 10-70° with a scanning step of 0.02° using Cu Kα radiation. The shape factor K is 0.89, X-ray wavelength of the Cu radiation is 0.1542 nm, B was obtained from Jade 5.0 (XRD analysis software) as FWHM values. Crystalline phase identification was carried out by comparison with the Joint Committee on Powder Diffraction Standards (JCPDS) standards.

3. Results and discussion

3.1. Characterizations of fresh NiO-Fe_2O_3-Al_2O_3 catalysts

3.1.1 N_2 adsorption analysis

Textural properties, theoretical metal composition, crystal size obtained from XRD analysis and BET surface area are shown in Table 1. The fresh co-precipitated NiO-Fe_2O_3-Al_2O_3 catalysts show relatively high BET surface areas ranging from 110.3 to 170.7m^2 g^{-1}. The specific BET surface area increased from 110.3 to 170.7 m^2 g^{-1}, then slightly decreased to 152.1m^2 g^{-1} when the Ni:Fe molar ratio was increased from 1:9 to 9:1. The surface area has been reported to be enhanced with the increase of Ni content by Yu et al. [30], who suggested that the increased fraction of spinel phase might contribute to the increase of BET surface area.

3.1.2. XRD analysis

XRD patterns of the fresh NiO-Fe_2O_3-Al_2O_3 catalysts are shown in Fig. 1 using the Joint Committee on Powder Diffraction Standards (JCPDS) file as a reference. The identifiable phases of the XRD patterns include $NiAl_2O_4$ (JCPDS 78-0552) and Ɣ-Al_2O_3 (29-0063) for all the fresh NiO-Fe_2O_3-Al_2O_3 catalysts. The diffraction peaks at 2θ of 31.4^o, 37.0^o, 45.0^o, 59.6^o and 65.5^o for stoichiometric $NiAl_2O_4$ spinel phase were clearly displayed as shown in Fig. 1. Chen et al. [31] reported that when Al^{3+} was rich in Ni-Al catalyst, Ni^{2+} coordinated with Al^{3+}

dominantly to form $NiAl_2O_4$ spinel phase. It is noted that Wang et al. [32] and López-Fonseca et al. [33] reported that diffraction lines for $NiAl_2O_4$ (JCPDS 78-0552) at 2θ positions (37.0°, 45.0°, 65.5°) overlap diffraction peaks of γ-Al_2O_3 at similar 2θ positions (37.6°, 45.8°, 66.8°), which was also observed in Fig. 1.

However, for the fresh NiO-Fe_2O_3-Al_2O_3 catalysts with Ni:Fe molar ratios of 9:1, 8:2, 6:4, 5:5 and 4:6, there were no clear evidence to prove the appearance of Fe species, which may result from the fact that the particle size of Fe species was too small to be detected [34]. In addition, it is also difficult to identify NiO particles; this might be also due to the presence of small NiO particles. By further increasing Fe content (the NiO-Fe_2O_3-Al_2O_3 catalyst with Ni:Fe molar ratio of 1:9), the diffraction lines of α-Fe_2O_3 (JCPDS 33-0664) at 2θ positions of 24.1°, 33.1°, 35.6°, 40.8°, 43.5°, 49.4°, 54.0°, 57.5° and γ-Fe_2O_3 (JCPDS 39-1346, 2θ=23.8°, 26.1°, 32.1°, 33.9°, 35.6°, 37.2°, 40.4°, 43.3°, 50.0°, 53.7°, 54.9°, 57.3°) were identified; this might be due to the increased content of Fe in the catalyst. The particle size for $NiAl_2O_4$ spinel calculated at the 2θ position of 45.0° and the particle size for γ-Al_2O_3 calculated at 65.5° in NiO-Fe_2O_3-Al_2O_3 catalyst were both about 5 nm.

3.1.3. SEM analysis

The SEM images of fresh NiO-Fe_2O_3-Al_2O_3 catalysts with scale bar of 1 um are shown in Fig. 2. With the change of Ni:Fe molar ratios, the morphology of catalysts only changed slightly with similar morphologies. The micrographs which can be seen from Fig. 2 show the presence of agglomerates composed of small quasi-spherical particles for all fresh NiO-Fe_2O_3-Al_2O_3 catalysts. However, due to the fact that the particle size of crystal phases in fresh NiO-Fe_2O_3-Al_2O_3 catalysts is only around 5nm (Obtained from XRD analysis and shown in Table 1), the particles of crystal phases are difficult to be observed using SEM analysis.

3.1.4. TEM analysis

The TEM images of the selected catalysts including the fresh 9Ni1FeAl, 5Ni5FeAl and 1Ni9FeAl catalysts are depicted in Fig. 3. A high dispersion of metal particles can be observed, with a homogeneous distribution in a form of small well-dispersed particles. The particle size obtained from TEM images is around 5nm which is in agreement with the XRD results (shown in Table 1) for both the fresh 9Ni1FeAl and 5Ni5FeAl catalysts. With the increase of Fe:Ni molar ratio to 9:1, the size of metal particles was increased significantly as shown in Fig. 3 (c).

However, it was impossible to distinguish $NiAl_2O_4$, α-Fe_2O_3, Y-Fe_2O_3 and Y-Al_2O_3 from the TEM analysis (Obtained from XRD results shown in Fig. 1).

3.1.5. TPR analysis

TPR analysis of fresh catalysts are shown in Fig. 4 to obtain the thermal stabilities of catalysts, and the interaction between metal and support. There is a wide H_2 consumption temperature window from 300 to 1050 °C with a maximum value at around 800 °C and two other smaller reduction peaks at approximate 420 and 550 °C, respectively, for all the fresh catalysts.

For the fresh NiO-Fe_2O_3-Al_2O_3 catalysts with a Ni:Fe molar ratio of 9:1, there is another extra small reduction peak at about 250 °C which might be attributed to the transformation from Fe_2O_3 to Fe_3O_4, which was also reported by other researchers [35].

Chen et al. [31] reported that the reduction peak at around 800 °C might be assigned as the reduction of stoichiometric $NiAl_2O_4$ spinel phase, which was also identified by the XRD results (Fig. 1) and other researchers [36, 37]. In addition, according to Ayub et al. [38] and Ratkovic et al. [39], the reduction peaks at around 420, 550 and 800 °C can be assigned as the reduction of γ-Fe_2O_3. The reduction of Fe-oxide species in the literature is usually reported as two- or three-step process (Fe_2O_3->Fe_3O_4->Fe or Fe_2O_3->Fe_3O_4->FeO->Fe) depending on the weight of the sample, composition of reducing agent and the particle size of metal oxides [40].

With the decrease of Ni content and the increase of Fe content, for example, when the Ni:Fe molar ratio was de~~in~~creased to 5:5, 4:6, 2:8 and 1:9, two small reduction peaks at around 420 and 550 °C were clearly observed. The maximum reduction temperature was slightly increased to 830 °C and the width of the peak was enhanced with the increase of Fe content, indicating more metal oxide species were reduced and the reducibility was reduced for the bimetallic catalysts [39].

3.2. Catalytic steam gasification of biomass

3.2.1. Mass balance

The yields of gas, solid residue and mass balance are presented in Table 2. The residue yield was around 36.3 wt.% for each experiment, since pyrolysis at the first stage was the same. It is noted that the amount of carbon formed inside the second reactor was negligible by weighting the reactor before and after the experiment. As mentioned previously, the liquid collected in the condensation system contains both unreacted water and oil, as the oil was not the key target

of this work, detailed oil analysis was not carried out. The mass balance showed that reliable results were obtained from the experiments to support discussions.

When the steam reforming of the derived vapours from pyrolysis of wood sawdust was carried out with a sand bed (as a 'blank' comparative material within the second reactor), the gas yield related to the mass of wood sawdust was 33.0 wt.%, and the hydrogen production was 2.4 mmol (H_2 g^{-1} wood sawdust). The production of hydrogen is calculated by the molar of hydrogen divided by the weight of the biomass sample used in each experiment. When the reforming process was performed with the addition of NiO-Fe_2O_3-Al_2O_3 catalysts, both the gas and hydrogen yields were enhanced significantly. For example, the gas yield was increased from 33.0 to 62.8 wt.% and the hydrogen production was increased from 2.4 to 11.4 (mmol H_2 g^{-1} wood sawdust). The highest gas and hydrogen yields were obtained with the 9Ni1FeAl catalyst, indicating that Ni played an important role for hydrogen and gas production in the process of catalytic steam thermo-chemical conversion of biomass.

The relationship between Ni content and catalytic reactivity have been investigated by other researchers. Barroso et al. [41] studied hydrogen production from steam reforming of ethanol using NiZnAl catalysts with different Ni loadings; it was reported that with the increase of Ni content, both the gas and hydrogen yields were increased. In our previous work, Ni/MCM41 catalysts with different Ni loadings ranging from 5 to 40 wt.% were used for catalytic thermo-chemical conversion of wood sawdust, also both the gas and hydrogen yields were increased with the increase of Ni loadings. It is therefore suggested that a well distributed and increased metal particle content (e.g. Ni) is one of the key factors to enhance hydrogen production from catalytic thermo-chemical conversion of hydrocarbons [42].

With the decrease of Ni content or increasing the Fe content, both gas and hydrogen yields were decreased and then increased, indicating that Fe content also influenced gas and hydrogen yields. According to Nordgreen et al. [21], metallic iron obtained by reducing iron oxides (FeO, Fe_2O_4 and Fe_3O_4) significantly reduced the content of tar, a mixture of hydrocarbons produced from biomass gasification. Kuhn et al. [43] investigated catalytic steam reforming of tar in the presence of olivine catalysts; they reported that Fe-related species increased significantly the production of hydrogen, compared to the experiment using only olivine. Similar contributions of Fe-related species to hydrogen production was also reported by Devi et al. [44], when catalytic steam reforming of naphthalene (a model biomass tar compound) was carried out.

As shown in Table 2, when the molar ratio of Ni:Fe was higher than 1, the gas and hydrogen yields were higher than the catalysts with the Ni: Fe molar ratio less than 1, indicating that Ni played a dominant role for hydrogen production compared to Fe, which is consistent with other literature [45]. It is suggested that Ni-species have high catalytic ability to break down C-H and C-C bonds compared to Fe-species.

With decreasing the Ni:Fe molar ratio from 9:1 to 2:8, both gas and H_2 yields were decreased. By further decreasing the Ni:Fe molar ratio, the gas and H_2 yields were increased slightly, but were still lower compared to the catalysts with the Ni:Fe molar ratio larger than 1. This might be ascribed to the presence of Fe oxides as shown in the XRD analysis (Fig. 1). Similar results have been reported by Wang et al. [28], in the steam reforming process of tar carried out with Ni-Fe/α-Al_2O_3 catalysts, the addition of Fe to Ni/α-Al_2O_3 promoted the steam reforming reaction monotonously in the range of the molar ratio of Fe to Ni(Fe/Ni)≤0.5, and the amount of tar decreased. In contrast, the excess addition of Fe (Fe/Ni>0.5) decreased the formation rate of gaseous products. High activity of Ni-Fe/α-Al_2O_3 catalysts can be caused by the synergy between Ni and Fe. It has been reported that Ni-Fe bimetallic catalysts derived from $LaNi_{0.3}Fe_{0.7}O_3$ were effective for the gasification of almond shell and steam reforming of methane [46].

3.2.2. Gas concentration

As shown in Table 2, when the pyrolysis and steam gasification process was carried out with a sand bed, the H_2 content was 17.4vol.%, CO content was 45.5vol.%, CO_2 content was 14.5vol.%, CH_4 content was 14.8vol.% while C_2-C_4 content was 7.8vol.%.

Compared with non-catalytic steam gasification of wood sawdust, the H_2 concentration was increased to 37.2vol.%, CO_2 concentration was enhanced to 21.3vol.% while CO, CH_4 and C_2-C_4 concentration were all decreased, to 27.4, 6.2 and 1.2vol.%, respectively, during the steam gasification process in the presence of NiO-Fe_2O_3-Al_2O_3 catalysts. This suggests that the water-gas shift reaction (Equation 5), reforming and decomposition of hydrocarbons and oxygenated compounds (Equation 4 to Equation 9) were possibly promoted with Ni-based catalysts, Fe-based catalysts and/or bimetallic Ni-Fe based catalysts [21, 28, 47, 48].

With the increase of Fe content, the CO composition in the catalytic performance of steam gasification process was firstly decreased from 41.6 to 27.4vol.%, then increased to 30.3vol.%. H_2 composition ranged from 37.2 to 32.7vol.%, CO_2 composition was increased from 14.5 to

21.3vol.%, both CH_4 and C_2-C_4 compositions were firstly increased then decreased, from 6.2 to 13.7vol.%, then to 12.1vol.% and from 1.2 to 4.1vol.%, then to 3.4vol.%, respectively.

$$Tar \rightarrow aCO + bCH_4 + cC \quad \text{Equation 1}$$

$$CO + H_2O \leftrightarrow CO_2 + H_2 \quad \text{Equation 2}$$

$$CH_4 + H_2O \leftrightarrow CO + 3H_2 \quad \text{Equation 3}$$

$$C_{(s)} + O_2 \leftrightarrow CO_2 \quad \text{Equation 4}$$

$$C_{(s)} + H_2O \leftrightarrow CO + H_2 \quad \text{Equation 5}$$

$$C_{(s)} + CO_2 \leftrightarrow 2CO \quad \text{Equation 6}$$

The decrease of CO fraction~~content~~ indicated that the water-gas shift reaction (Equation 5) was enhanced by the addition of catalysts. The lowest CO content was generated with the 5Ni5FeAl catalyst, indicating the water-gas shift reaction (Equation 5) was promoted to the largest extent in the presence of the 5Ni5FeAl catalyst. In addition, when the Ni:Fe molar ratio was larger than 1, the contents of CO_2, CH_4 and C_2-C_4 content were smaller than that produced with Ni:Fe ratio smaller than 1, indicating there was an optimal addition of Fe-species for the promotion of water-gas shift reaction (Equation 5) and hydrocarbon decomposition reaction (Equation 6). However, the H_2 composition was higher when the Ni:Fe molar ratio was larger than 1. Thus it is suggested that hydrogen production was mainly contributed by Ni-species in the NiO-Fe_2O_3-Al_2O_3 catalyst.

According to gas composition data in Table 2 and Fig. 5, although the highest gas and H_2 yields were obtained with the 9Ni1FeAl catalyst, the highest H_2/CO ratio, and lowest CO/CO_2 ratio were obtained with the utilization of the 5Ni5FeAl catalyst. The H_2/CO molar ratio showed a trend of an initial increase from 0.4 to 1.3, and then decreased to 1.1, when the Ni:Fe ratio was reduced from 9:1 to 1:9; while the CO/CO_2 molar ratio has an opposite trend, which was firstly decreased from 3.1 to 1.3, then increased to 1.5. It is demonstrated that the increase of Fe content promoted the water-gas shift reaction (Equation 5) and this reaction was promoted to the largest extent when the 5Ni5FeAl catalyst was present in the steam gasification process.

Polychronopoulou et al. [49] investigated an adsorption-enhanced steam reforming process of phenol (a model compound of wood biomass pyrolysis oil) carried out with supported Fe catalysts, the optimum loading of Fe for maximum H_2 yield was 5 wt.%. According to Orío et al. [42], four different dolomites with varying Fe_2O_3 content were investigated for oxygen/steam

gasification of wood, the dolomite with highest Fe_2O_3 content exhibited the highest activity with 95% tar conversion.

Based on the research work of Wang et al. [32], the catalytic performance of NiO-Fe_2O_3-Al_2O_3 catalyst for partial oxidation showed that the conversion of methane and the selectivity of CO and H_2 were 90.09, 97.28 and 97.09%, respectively at 875°C. According to Wang et al. [50], the utilization of co-precipitated Ni-Fe catalysts for hydrogen production from partial oxidation of ethanol (a model compound of biomass derived by-product) was performed, the $Ni_{50}Fe_{50}$ catalyst showed the best activity in terms of the ethanol conversion and the selectivity of hydrogen.

3.2.3. Coke deposition on used catalysts

The used catalysts were characterized by TPO analysis and the results are shown in Fig. 6 via weight change intensity (mg) versus temperature (°C). Two oxidation stages in the TPO analysis are observed, the first oxidation peak is ascribed to the oxidation of metal particles and the second peak was for carbon oxidation. The peaks of increasing mass from 300 to 600°C and above 700°C were associated with the oxidation of Ni and Fe species during the TPO analysis. The reduced metal species were suggested to be produced during the pyrolysis and steam reforming process where reduction agent H_2 and CO were present [29]. Therefore, the reduction of fresh catalysts before the reaction is unnecessary, which reduced the operation cost.

Weight loss before 550°C for the TPO analysis is suggested to be assigned to the oxidation of amorphous carbon. The oxidation peak at a higher temperature which starts from 550 to 700°C might be attributed to the oxidation of filamentous carbon deposited on the surface of the reacted catalyst [51]. The amount of coke formation was calculated as the weight loss except for the oxidation of metal divided by the initial sample weight during the TPO experiment. It is proposed that the total amount of coke deposition on the used catalyst was less than 2wt.% in relation to the weight of the used catalyst with a Ni:Fe molar ratio of 1:9, indicating that a high stability of catalyst resistant to coke deposition. At the temperature of 800°C, carbon gasification reaction and Boudouard reaction (Equation 8 and Equation 9) contribute to the reduction of coke formation as suggested by Sutton et al. [42]. Corujo et al. [52] reported a more than 5 wt.% amount of coke formation on a Ni/dolomite catalyst for steam gasification of forestry residue and an even higher amount (>10wt.%) of coke formation was obtained on a reacted Ni/Al_2O_3 catalyst for the steam gasification of biomass reported by Nishikawa et al. [53].

SEM analysis, shown in Fig. 7, confirms the presence of amorphous and filamentous carbon on the surface of the used catalysts with a Ni:Fe ratio larger than 1 and there was almost no carbon deposition on the surface for the reacted catalysts with a Ni:Fe ratio smaller than 1. Wang et al. [28] reported that one of the drawbacks of using Ni-based catalysts during steam reforming of biomass tar was carbon deposition on the surface of metallic Ni species, while Ni-Fe alloy species could resist the formation of coke. Therefore, they reported the addition of Fe suppressed the carbon deposition on the surface of the reacted catalyst. ~~The more accurate analysis is suggested to differentiate the oxidation of metal and carbon in future work, e.g. using TPO-FTIR method.~~

Although the filamentous carbon was confirmed by the SEM images, due to the low amount of coke deposited on the used catalyst, it was not identified from the TEM analysis as shown in Fig. 8. TEM analysis of the size of metal particle (~4 nm) inside the reacted 9Ni1FeAl (Fig. 8) was similar to the results shown in Fig. 3 (fresh catalyst), indicating sintering was not serious after the catalytic reforming of vapour produced from pyrolysis of sawdust.

Conclusions

In this work, NiO-Fe_2O_3-Al_2O_3 catalysts with different Ni:Fe molar ratios (9:1, 8:2, 6:4, 5:5, 4:6, 2:8 and 1:9) prepared by co-precipitation method have been investigated for hydrogen-rich syngas production from pyrolysis and steam reforming of wood sawdust. ~~The main outcomes were:~~

~~(1)~~ The prepared catalyst has well-dispersed $NiAl_2O_4$, α-Fe_2O_3 and γ-Fe_2O_3 crystal phases. The high dispersion of metal species was proved to enhance the catalyst stability in terms of coke formation on the surface of the used catalyst and the sintering of metal particles.

~~(2)~~ Both gas and hydrogen yields were increased significantly when catalysts were added into the gasification process, gas production was increased from 33.0 to 62.8 wt.% and the H_2 yield was enhanced from 2.4 to 11.4 $mmol g^{-1}$wood sawdust with the 9Ni1FeAl catalyst.~~;~~

~~(3)~~ The enhanced hydrogen production was suggested to be due to the increased number of catalytic sites during the biomass gasification process and both Ni and Fe metal (mainly Ni) promoted the steam gasification process. ~~;~~

(4) Coke deposition on the reacted 1Ni9FeAl catalyst (<2wt.%) was suggested to be negligible. The increase of Fe addition to the NiO-Fe_2O_3-Al_2O_3 significantly reduced the amount of coke formed on the surface of the catalyst, as obtained from the TPO analysis of the reacted catalyst.

Acknowledgement

This work was supported by the International Exchange Scheme from the Royal Society (IE110273), UK, the Australian Research Council DP150103842, and the Early Career Research Scheme and MCR from the University of Sydney.

References

1. Renewables 2010 Global Status Report from the Renewable Energy Policy Network for the 21st Century, extracted on 15th, March, 2014, http://www.mofa.go.jp/mofaj/gaiko/energy/irena/workshop1102/pdfs/pdf3.pdf.

2. Wu, C.; Wang, L.; Williams, P. T.; Shi, J.; Huang, J., Hydrogen production from biomass gasification with Ni/MCM-41 catalysts: Influence of Ni content. *Applied Catalysis B: Environmental* **2011,** 108–109, (0), 6-13.

3. Lv, P.; Chang, J.; Wang, T.; Fu, Y.; Chen, Y.; Zhu, J., Hydrogen-Rich Gas Production from Biomass Catalytic Gasification. *Energy & Fuels* **2003,** 18, (1), 228-233.

4. Wu, C.; Williams, P. T., Hydrogen production by steam gasification of polypropylene with various nickel catalysts. *Applied Catalysis B: Environmental* **2009,** 87, (3–4), 152-161.

5. *Renewables 2011: Global Status Report, extracted on 15th, March, 2014, http://germanwatch.org/klima/gsr2011.pdf*.

6. Sutton, D.; Kelleher, B.; Ross, J. R. H., Review of literature on catalysts for biomass gasification. *Fuel Processing Technology* **2001,** 73, (3), 155-173.

7. Inaba, M.; Murata, K.; Saito, M.; Takahara, I., Hydrogen Production by Gasification of Cellulose over Ni Catalysts Supported on Zeolites. *Energy & Fuels* **2006,** 20, (2), 432-438.

8. Wu, C.; Williams, P. T., Ni/CeO2/ZSM-5 catalysts for the production of hydrogen from the pyrolysis–gasification of polypropylene. *International Journal of Hydrogen Energy* **2009,** 34, (15), 6242-6252.

9. Deng, X.; Sun, J.; Yu, S.; Xi, J.; Zhu, W.; Qiu, X., Steam reforming of ethanol for hydrogen production over NiO/ZnO/ZrO2 catalysts. *International Journal of Hydrogen Energy* **2008,** 33, (3), 1008-1013.

10. Piscina, P. R. d. l.; Homs, N., Use of biofuels to produce hydrogen (reformation processes). *Chemical Society Reviews* **2008,** 37, (11), 2459-2467.

11. Devi, L.; Ptasinski, K. J.; Janssen, F. J. J. G., A review of the primary measures for tar elimination in biomass gasification processes. *Biomass Bioenergy* **2003,** 24, (Copyright (C) 2012 American Chemical Society (ACS). All Rights Reserved.), 125-140.

12. Nakamura, K.; Miyazawa, T.; Sakurai, T.; Miyao, T.; Naito, S.; Begum, N.; Kunimori, K.; Tomishige, K., Promoting effect of MgO addition to Pt/Ni/CeO2/Al2O3 in the steam gasification of biomass. *Applied Catalysis B: Environmental* **2009,** 86, (1–2), 36-44.

13. Tomishige, K.; Asadullah, M.; Kunimori, K., Syngas production by biomass gasification using Rh/CeO2/SiO2 catalysts and fluidized bed reactor. *Catalysis Today* **2004,** 89, (4), 389-403.

14. Wu, C.; Williams, P. T., Investigation of Ni-Al, Ni-Mg-Al and Ni-Cu-Al catalyst for hydrogen production from pyrolysis–gasification of polypropylene. *Applied Catalysis B: Environmental* **2009,** 90, (1–2), 147-156.

15. Corujo, A.; Yermán, L.; Arizaga, B.; Brusoni, M.; Castiglioni, J., Improved yield parameters in catalytic steam gasification of forestry residue; optimizing biomass feed rate and catalyst type. *Biomass and Bioenergy* **2010,** 34, (12), 1695-1702.

16. Wu, C.; Wang, Z.; Huang, J.; Williams, P. T., Pyrolysis/gasification of cellulose, hemicellulose and lignin for hydrogen production in the presence of various nickel-based catalysts. *Fuel* **2013,** 106, (0), 697-706.

17. Miyazawa, T.; Kimura, T.; Nishikawa, J.; Kado, S.; Kunimori, K.; Tomishige, K., Catalytic performance of supported Ni catalysts in partial oxidation and steam reforming of tar derived from the pyrolysis of wood biomass. *Catalysis Today* **2006,** 115, (1–4), 254-262.

18. Kimura, T.; Miyazawa, T.; Nishikawa, J.; Kado, S.; Okumura, K.; Miyao, T.; Naito, S.; Kunimori, K.; Tomishige, K., Development of Ni catalysts for tar removal by steam gasification of biomass. *Applied Catalysis B: Environmental* **2006,** 68, (3–4), 160-170.

19. Tomishige, K.; Kimura, T.; Nishikawa, J.; Miyazawa, T.; Kunimori, K., Promoting effect of the interaction between Ni and CeO2 on steam gasification of biomass. *Catalysis Communications* **2007,** 8, (7), 1074-1079.

20. Nishikawa, J.; Nakamura, K.; Asadullah, M.; Miyazawa, T.; Kunimori, K.; Tomishige, K., Catalytic performance of Ni/CeO2/Al2O3 modified with noble metals in steam gasification of biomass. *Catalysis Today* **2008,** 131, (1–4), 146-155.

21. Nordgreen, T.; Liliedahl, T.; Sjöström, K., Metallic iron as a tar breakdown catalyst related to atmospheric, fluidised bed gasification of biomass. *Fuel* **2006,** 85, (5–6), 689-694.

22. Devi, L.; Craje, M.; Thüne, P.; Ptasinski, K. J.; Janssen, F. J. J. G., Olivine as tar removal catalyst for biomass gasifiers: Catalyst characterization. *Applied Catalysis A: General* **2005,** 294, (1), 68-79.

23. Devi, L.; Ptasinski, K. J.; Janssen, F. J. J. G., A review of the primary measures for tar elimination in biomass gasification processes. *Biomass and Bioenergy* **2003,** 24, (2), 125-140.

24. Devi, L.; Ptasinski, K. J.; Janssen, F. J. J. G., Pretreated olivine as tar removal catalyst for biomass gasifiers: investigation using naphthalene as model biomass tar. *Fuel Processing Technology* **2005,** 86, (6), 707-730.

25. Devi, L.; Ptasinski, K. J.; Janssen, F. J. J. G.; van Paasen, S. V. B.; Bergman, P. C. A.; Kiel, J. H. A., Catalytic decomposition of biomass tars: use of dolomite and untreated olivine. *Renewable Energy* **2005,** 30, (4), 565-587.

26. Ramli, A.; Misi, S. E. E.; Mohamad, M. F.; Yusup, S. In *Hydrogen Production from Steam Gasification of Palm Kernel Shell Using Sequential Impregnation Bimetallic Catalysts*, The 2013 International Conference on Environment, Energy, Ecosystems and Development, Rhodes (Rodos) Island, Greece, 2013; Rhodes (Rodos) Island, Greece, 2013; pp 177-181.

27. Wang, W.; Wang, Z.; Ding, Y.; Xi, J.; Lu, G., Partial Oxidation of Ethanol to Hydrogen over Ni–Fe Catalysts. *Catalysis Letters* **2002,** 81, (1-2), 63-68.

28. Wang, L.; Li, D.; Koike, M.; Koso, S.; Nakagawa, Y.; Xu, Y.; Tomishige, K., Catalytic performance and characterization of Ni-Fe catalysts for the steam reforming of tar from biomass pyrolysis to synthesis gas. *Applied Catalysis A: General* **2011,** 392, (1–2), 248-255.

29. Wu, C.; Wang, L.; Williams, P. T.; Shi, J.; Huang, J., Hydrogen production from biomass gasification with Ni/MCM-41 catalysts: Influence of Ni content. *Appl. Catal., B* **2011,** 108–109, (0), 6-13.

30. Yu, Z.; Chen, D.; Rønning, M.; Vrålstad, T.; Ochoa-Fernández, E.; Holmen, A., Large-scale synthesis of carbon nanofibers on Ni–Fe–Al hydrotalcite derived catalysts: I. Preparation and characterization of the Ni–Fe–Al hydrotalcites and their derived catalysts. *Appl. Catal., A* **2008,** 338, (1–2), 136-146.

31. Chen, J.; Qiao, Y.; Li, Y., Modification of Ni state to promote the stability of Ni–Al_2O_3 catalyst in methane decomposition to produce hydrogen and carbon nanofibers. *J. Solid State Chem.* **2012,** 191, (0), 107-113.

32. Wang, J.-g.; Liu, C.-j.; Zhang, Y.-p.; Yu, K.-l.; Zhu, X.-l.; He, F., Partial oxidation of methane to syngas over glow discharge plasma treated Ni–Fe/Al_2O_3 catalyst. *Catal. Today* **2004,** 89, (1–2), 183-191.

33. López-Fonseca, R.; Jiménez-González, C.; de Rivas, B.; Gutiérrez-Ortiz, J. I., Partial oxidation of methane to syngas on bulk $NiAl_2O_4$ catalyst. Comparison with alumina supported nickel, platinum and rhodium catalysts. *Appl. Catal., A* **2012,** 437–438, (0), 53-62.

34. Wang, J.; Wu, W.; Zhao, F.; Zhao, G., Suppression of the Néel temperature in hydrothermally synthesized alpha-Fe_2O_3 nanoparticles. *J. Appl. Phys.* **2011,** 109, (5), 056101.

35. Lohitharn, N.; Goodwin Jr, J. G.; Lotero, E., Fe-based Fischer–Tropsch synthesis catalysts containing carbide-forming transition metal promoters. *J. Catal.* **2008,** 255, (1), 104-113.

36. Li, G.; Hu, L.; Hill, J. M., Comparison of reducibility and stability of alumina-supported Ni catalysts prepared by impregnation and co-precipitation. *Applied Catalysis A: General* **2006,** 301, (1), 16-24.

37. Zhang, J.; Xu, H.; Jin, X.; Ge, Q.; Li, W., Characterizations and activities of the nano-sized Ni/Al2O3 and Ni/La–Al2O3 catalysts for NH3 decomposition. *Applied Catalysis A: General* **2005,** 290, (1–2), 87-96.

38. Ayub, I.; Berry, F. J.; Crabb, E.; Helgason, Ö., Titanium-doped γ-Fe_2O_3: Reduction and oxidation properties. *J. Mater. Sci.* **2004,** 39, (23), 6921-6927.

39. Ratkovic, S.; Vujicic, D.; Kiss, E.; Boskovic, G.; Geszti, O., Different degrees of weak metal–support interaction in Fe–(Ni)/Al_2O_3 catalyst governing activity and selectivity in carbon nanotubes' production using ethylene. *Mater. Chem. Phys.* **2011,** 129, (1–2), 398-405.

40. Zieliński, J.; Zglinicka, I.; Znak, L.; Kaszkur, Z., Reduction of Fe_2O_3 with hydrogen. *Appl. Catal., A* **2010,** 381, (1–2), 191-196.

41. Barroso, M. N.; Gomez, M. F.; Arrúa, L. A.; Abello, M. C., Hydrogen production by ethanol reforming over NiZnAl catalysts. *Appl. Catal., A* **2006,** 304, (0), 116-123.

42. Sutton, D.; Kelleher, B.; Ross, J. R. H., Review of literature on catalysts for biomass gasification. *Fuel Process. Technol.* **2001,** 73, (3), 155-173.

43. Kuhn, J. N.; Zhao, Z.; Felix, L. G.; Slimane, R. B.; Choi, C. W.; Ozkan, U. S., Olivine catalysts for methane- and tar-steam reforming. *Appl. Catal., B* **2008,** 81, (1–2), 14-26.
44. Devi, L.; Craje, M.; Thüne, P.; Ptasinski, K. J.; Janssen, F. J. J. G., Olivine as tar removal catalyst for biomass gasifiers: Catalyst characterization. *Appl. Catal., A* **2005,** 294, (1), 68-79.
45. Ahmed, S.; Aitani, A.; Rahman, F.; Al-Dawood, A.; Al-Muhaish, F., Decomposition of hydrocarbons to hydrogen and carbon. *Appl. Catal., A* **2009,** 359, (1–2), 1-24.
46. Rapagná, S.; Provendier, H.; Petit, C.; Kiennemann, A.; Foscolo, P. U., Development of catalysts suitable for hydrogen or syn-gas production from biomass gasification. *Biomass Bioenergy* **2002,** 22, (5), 377-388.
47. Kimura, T.; Miyazawa, T.; Nishikawa, J.; Kado, S.; Okumura, K.; Miyao, T.; Naito, S.; Kunimori, K.; Tomishige, K., Development of Ni catalysts for tar removal by steam gasification of biomass. *Appl. Catal., B* **2006,** 68, (3–4), 160-170.
48. Wu, C.; Williams, P. T., Hydrogen production by steam gasification of polypropylene with various nickel catalysts. *Appl. Catal., B* **2009,** 87, (3–4), 152-161.
49. Polychronopoulou, K.; Bakandritsos, A.; Tzitzios, V.; Fierro, J. L. G.; Efstathiou, A. M., Absorption-enhanced reforming of phenol by steam over supported Fe catalysts. *J. Catal.* **2006,** 241, (1), 132-148.
50. Wang, W.; Wang, Z.; Ding, Y.; Xi, J.; Lu, G., Partial Oxidation of Ethanol to Hydrogen over Ni–Fe Catalysts. *Catal. Lett.* **2002,** 81, (1-2), 63-68.
51. Zeng, G.; Liu, Q.; Gu, R.; Zhang, L.; Li, Y., Synergy effect of MgO and ZnO in a Ni/Mg–Zn–Al catalyst during ethanol steam reforming for H_2-rich gas production. *Catal. Today* **2011,** 178, (1), 206-213.
52. Corujo, A.; Yermán, L.; Arizaga, B.; Brusoni, M.; Castiglioni, J., Improved yield parameters in catalytic steam gasification of forestry residue; optimizing biomass feed rate and catalyst type. *Biomass Bioenergy* **2010,** 34, (12), 1695-1702.
53. Nishikawa, J.; Miyazawa, T.; Nakamura, K.; Asadullah, M.; Kunimori, K.; Tomishige, K., Promoting effect of Pt addition to $Ni/CeO_2/Al_2O_3$ catalyst for steam gasification of biomass. *Catal. Commun.* **2008,** 9, (2), 195-201.

Table 1: Textural characteristics of fresh NiO-Fe_2O_3-Al_2O_3 catalysts.

Sample	Molar ratio (Ni:Fe)	Theoretical Metal Composition (wt.%)[a]			Particle size(nm)[b]		BET surface area (m^2/g)
		Ni	Fe	Al_2O_3	$NiAl_2O_4$	Y-Al_2O_3	
1Ni9FeAl	1:9	2.3	19.3	78.4	-	-	110.3
2Ni8FeAl	2:8	4.5	17.2	78.3	5.0	3.5	123.5
4Ni6FeAl	4:6	9.0	12.8	78.2	4.2	3.4	141.2
5Ni5FeAl	5:5	11.2	10.7	78.1	4.4	3.6	146.5
6Ni4FeAl	6:4	13.5	8.5	78.0	4.5	5.3	141.8
8Ni2FeAl	8:2	17.9	4.3	77.8	4.7	4.4	170.7
9Ni1FeAl	9:1	20.1	2.2	77.7	4.5	4.4	152.1

[a]The theoretical metal composition was calculated via the equation M=M/(Ni+Fe+Al_2O_3), where M represents Ni or Fe (wt.%).

[b]The particle size was calculated based on XRD result shown in Figure 5-1.

Table 2: Mass balance and gas compositions from pyrolysis and steam gasification of wood sawdust.

Catalyst bed	Sand	9Ni1FeAl	8Ni2FeAl	6Ni4FeAl	5Ni5FeAl	4Ni6FeAl	2Ni8FeAl	1Ni9FeAl
Gas/Wood sawdust (wt.%)	33.0	62.8	57.1	58.4	51.3	49.6	50.0	53.2
Residue/Wood (wt.%)	38.8	37.5	36.3	36.3	36.3	37.5	36.3	36.3
Mass balance (wt.%)	103.3	100.6	102.4	88.5	99.2	99.4	97.6	101.8
H_2 yield (mmol H^2g^{-1} wood)	2.4	11.4	10.7	9.2	8.7	8.4	7.7	8.3
Gas composition (vol.%, N_2 free)								
CO	45.5	41.6	32.9	38.0	27.4	28.0	30.3	29.8
H_2	17.4	36.5	37.2	33.6	35.2	34.8	32.7	33.4
CO_2	14.5	14.5	17.6	18.3	20.9	20.4	19.9	21.3
CH_4	14.8	6.2	10.3	8.0	13.4	13.7	12.9	12.1
C_2-C_4	7.8	1.2	2.1	2.1	3.1	3.1	4.1	3.4

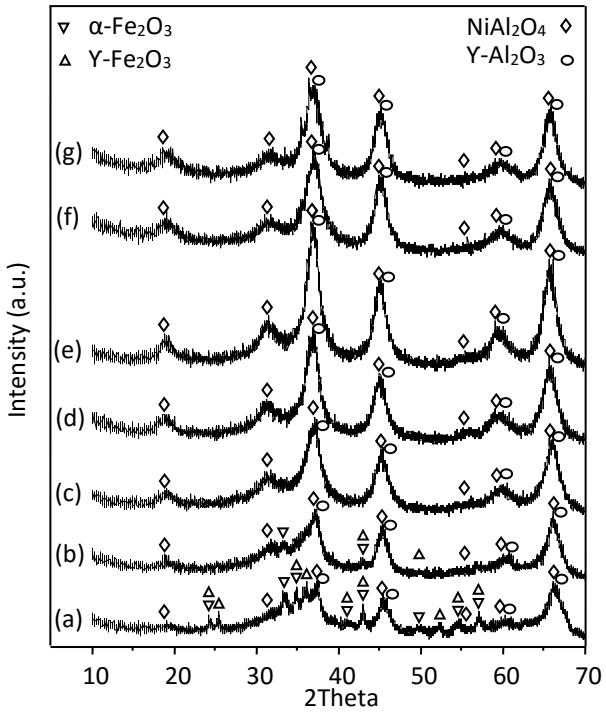

Fig. 1: XRD results for fresh NiO-Fe_2O_3-Al_2O_3 catalysts with different Ni:Fe ratios; (a): 1:9; (b): 2:8; (c): 4:6; (d): 5:5; (e): 6:4; (f): 8:2; (g): 9:1.

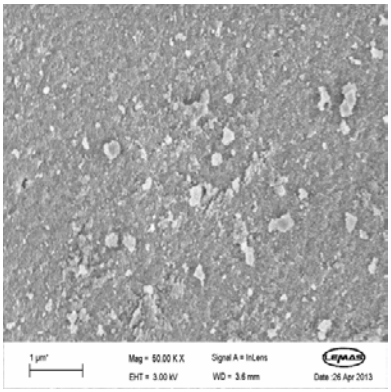

(a): Ni:Fe = 9:1;

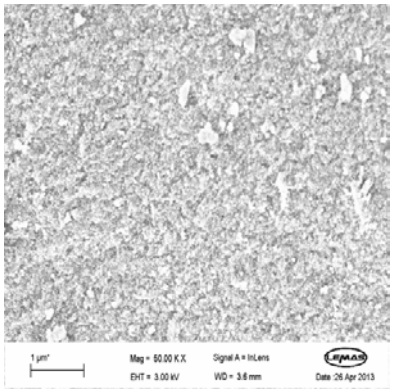

(b): Ni:Fe = 8:2;

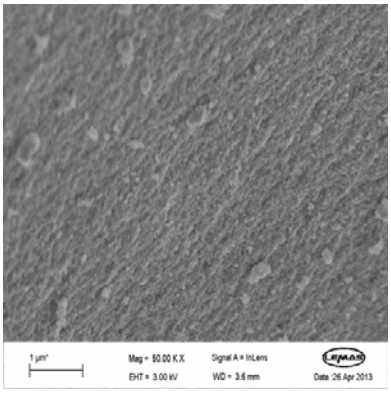

(c): Ni:Fe = 6:4;

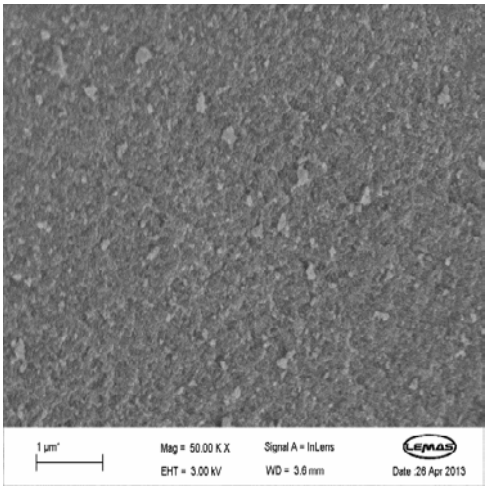

(d): Ni:Fe = 5:5;

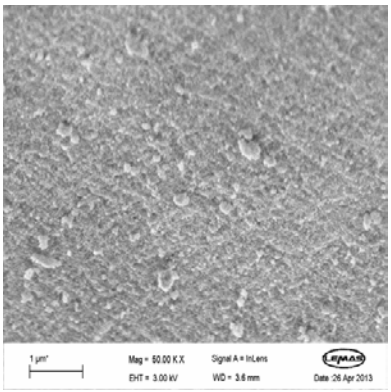

(e): Ni:Fe = 4:6;

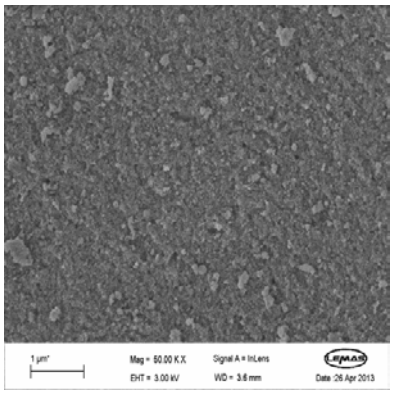

(f): Ni:Fe = 2:8;

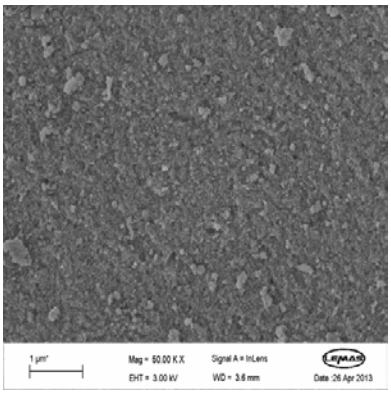

(g): Ni:Fe = 1:9.

Fig. 2: SEM results of fresh NiO-Fe_2O_3-Al_2O_3 catalysts with various Ni:Fe ratios.

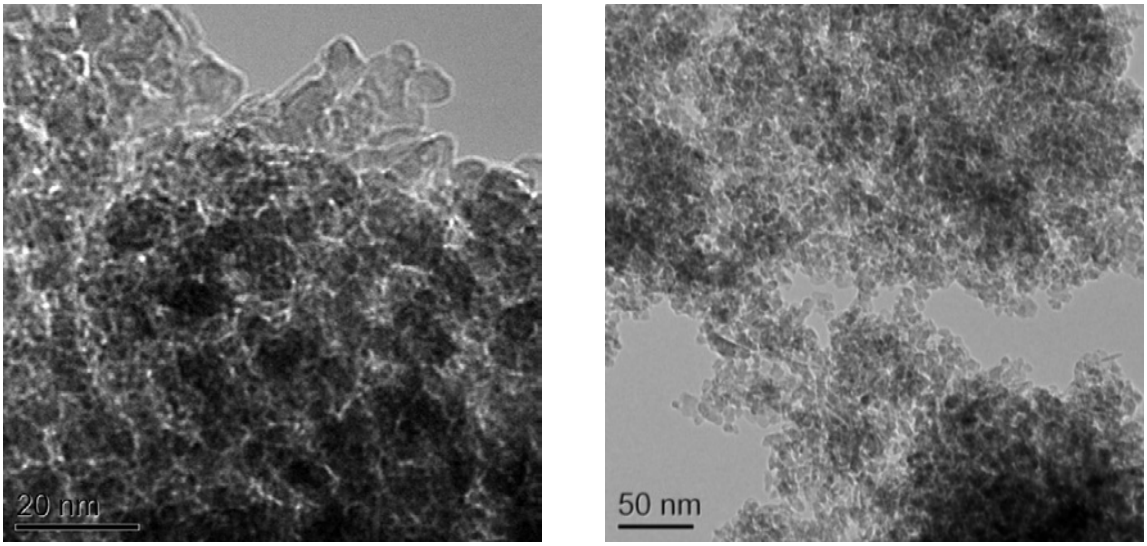

(a): fresh NiO-Fe_2O_3-Al_2O_3 catalyst with a Ni:Fe = 9:1;

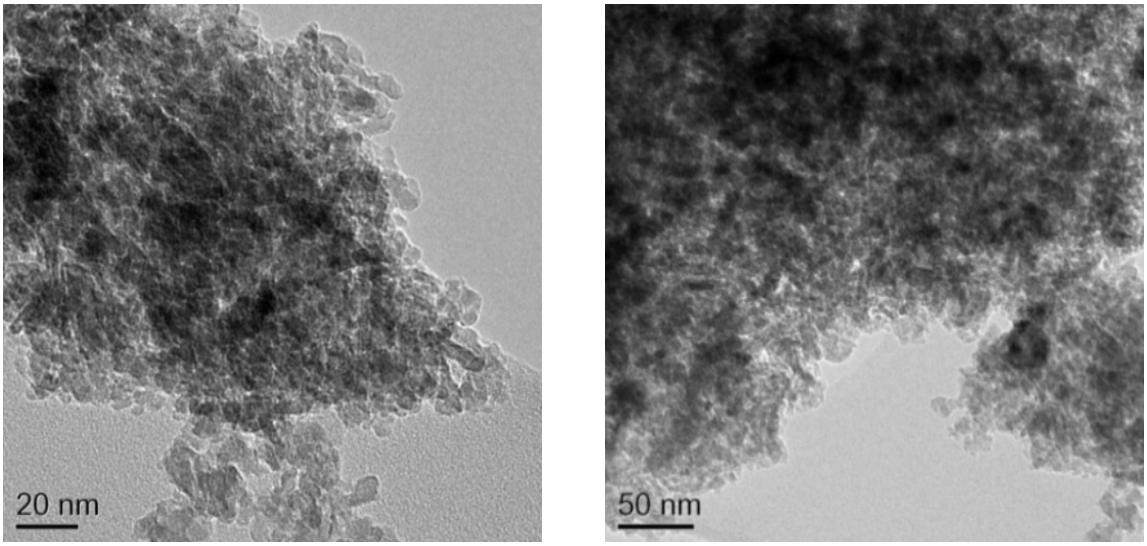

(b): fresh NiO-Fe_2O_3-Al_2O_3 catalyst with a Ni:Fe = 5:5;

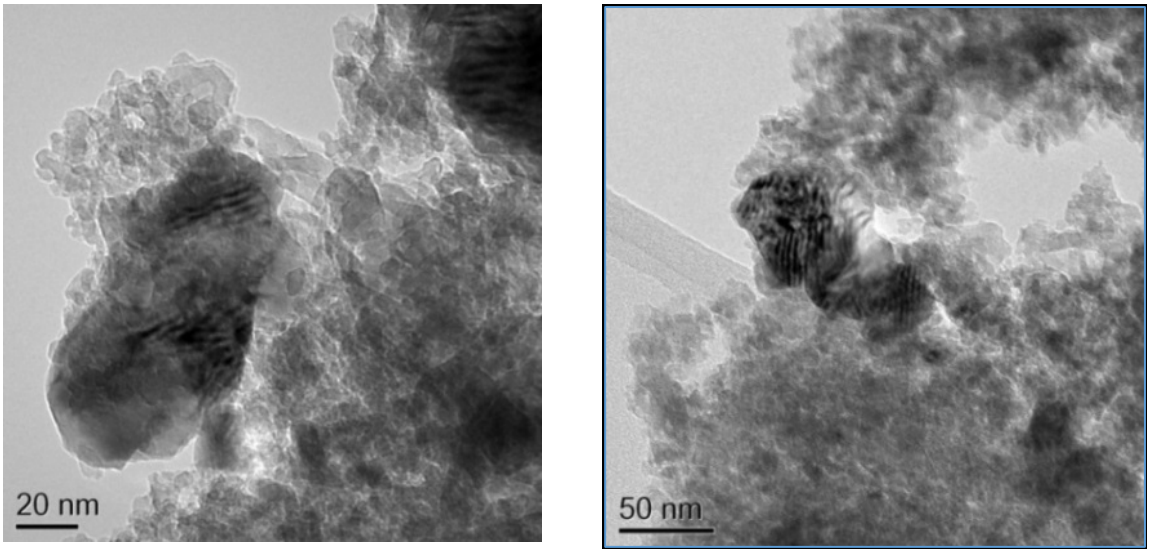

(c): fresh NiO-Fe_2O_3-Al_2O_3 catalyst with a Ni:Fe = 1:9.

Fig. 3: TEM analysis results of fresh NiO-Fe_2O_3-Al_2O_3 catalysts with various Ni:Fe molar ratios.

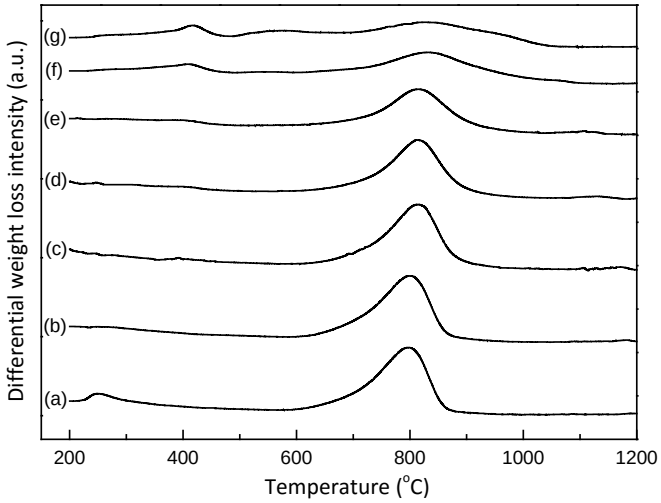

Fig. 4: Differentiated weight loss intensity results of fresh NiO-Fe_2O_3-Al_2O_3 catalysts with different Ni:Fe ratios; (a): 9:1; (b): 8:2; (c): 6:4; (d): 5:5; (e): 4:6; (f): 2:8; (g): 1:9.

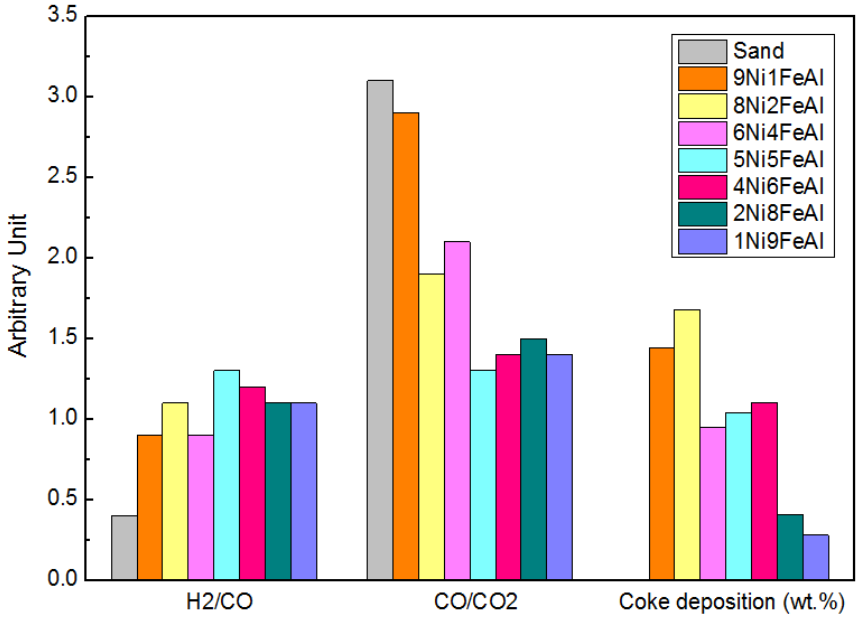

Fig. 5: H_2/CO, CO/CO_2 molar ratios based on gas composition in Table 2 and coke deposition based on TPO results in Fig.6.

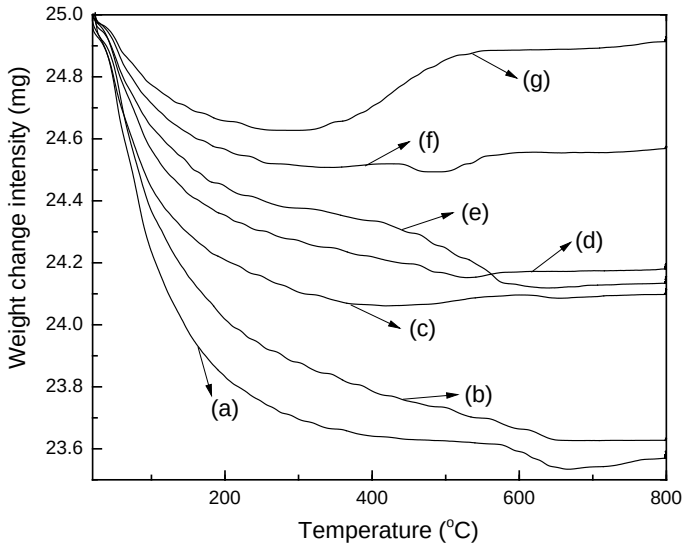

Fig. 6: Weight change intensity of used NiO-Fe_2O_3-Al_2O_3 catalysts with different Ni:Fe ratios; (a): 9:1; (b): 8:2; (c): 6:4; (d): 5:5; (e): 4:6; (f): 2:8; (g): 1:9.

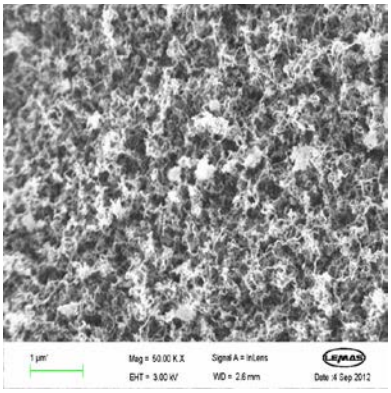

(a): used, Ni:Fe = 9:1;

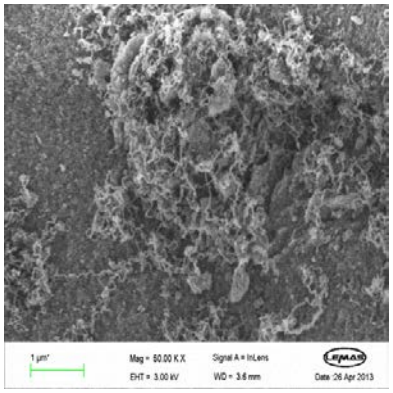

(b): used, Ni:Fe = 8:2;

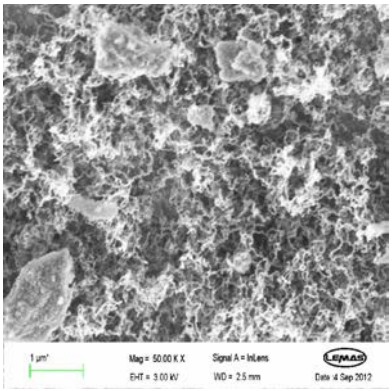

(c): used, Ni:Fe = 6:4;

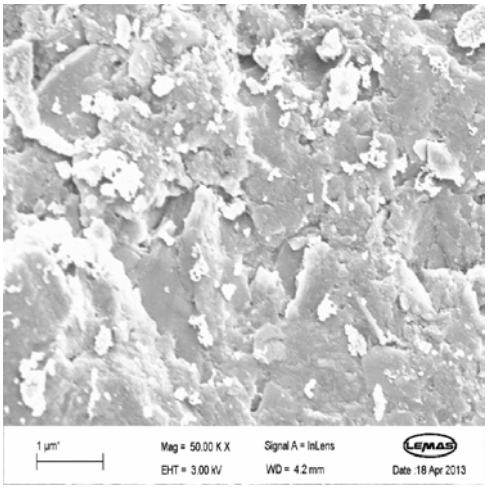

(d): used, Ni:Fe = 5:5;

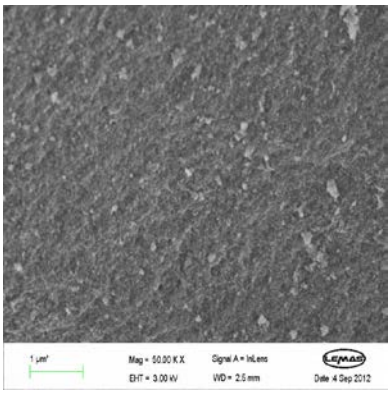

(e): used, Ni:Fe = 4:6;

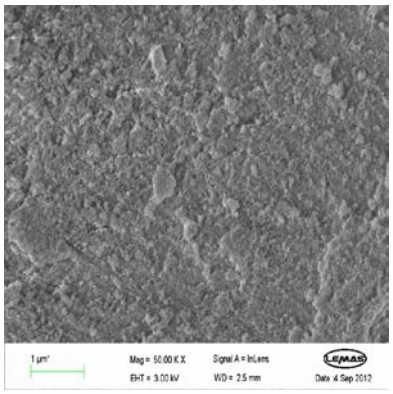

(f): used, Ni:Fe = 2:8;

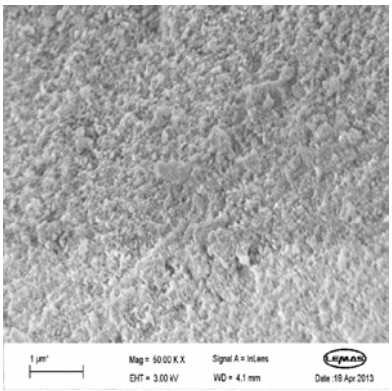

(g): used, Ni:Fe = 1:9.

Fig. 7: SEM results of used NiO-Fe_2O_3-Al_2O_3 catalysts with various Ni:Fe ratios.

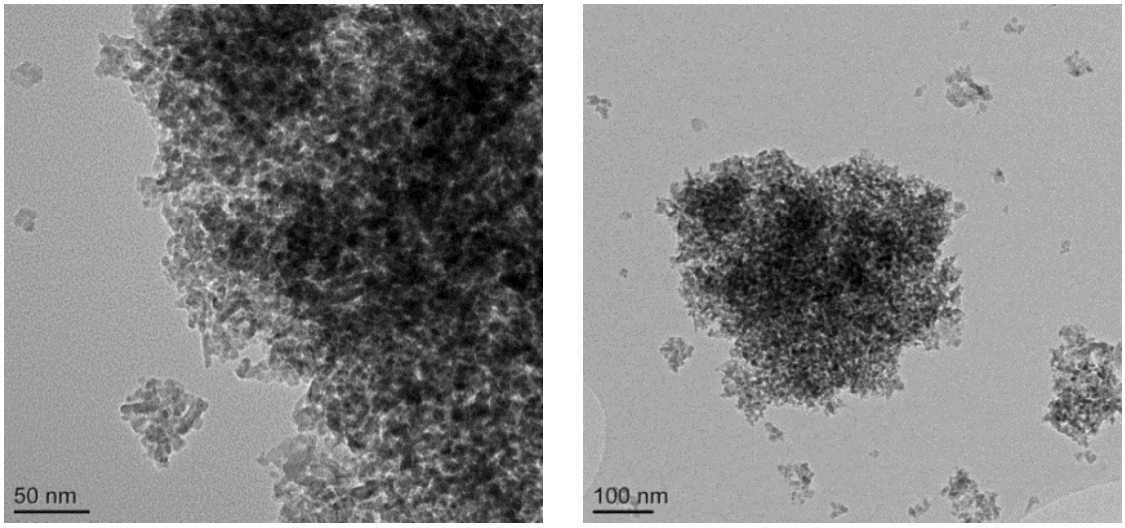

Fig. 8: TEM results of used NiO-Fe_2O_3-Al_2O_3 catalysts with a Ni:Fe molar ratio of 9:1.